
Symmetric Variational Autoencoder and Connections to Adversarial Learning

Yunchen Pu, Liqun Chen, Shuyang Dai, Weiyao Wang, Chunyuan Li, Lawrence Carin

Department of Electrical and Computer Engineering, Duke University

{yunchen.pu, liqun.chen, shuyang.dai, weiyao.wang2, chunyuan.li, lcarin}@duke.edu

Abstract

A new form of the variational autoencoder (VAE) is proposed, based on the *symmetric* Kullback-Leibler divergence. It is demonstrated that learning of the resulting symmetric VAE (sVAE) has close connections to previously developed adversarial-learning methods. This relationship helps unify the previously distinct techniques of VAE and adversarial learning, and provides insights that allow us to ameliorate shortcomings with some previously developed adversarial methods. In addition to an analysis that motivates and explains the sVAE, an extensive set of experiments validate the utility of the approach.

1 Introduction

Generative models that are *descriptive* of data have been widely employed in statistics and machine learning. Factor models (FMs) represent one commonly used generative model [25], and mixtures of FMs have been employed to account for more-general data distributions [7]. These models typically have latent variables (e.g., factor scores) that are inferred given observed data; the latent variables are often used for a down-stream goal, such as classification [5]. After training, such models are useful for inference tasks given subsequent observed data. However, when one draws from such models, by drawing latent variables from the prior and pushing them through the model to synthesize data, the synthetic data typically do not appear to be realistic. This suggests that while these models may be useful for analyzing observed data in terms of inferred latent variables, they are also capable of describing a large set of data that do not appear to be real.

The generative adversarial network (GAN) [9] represents a significant recent advance toward development of gen-

erative models that are capable of synthesizing realistic data. Such models also employ latent variables, drawn from a simple distribution analogous to the aforementioned prior, and these random variables are fed through a (deep) neural network. The neural network acts as a functional transformation of the original random variables, yielding a model capable of representing sophisticated distributions. Adversarial learning discourages the network from yielding synthetic data that are unrealistic, from the perspective of a learned neural-network-based classifier. However, GANs are notoriously difficult to train, and multiple generalizations and techniques have been developed to improve learning performance [22], for example Wasserstein GAN (WGAN) [1, 2] and energy-based GAN (EB-GAN) [29].

While the original GAN and variants were capable of synthesizing highly realistic data (e.g., images), the models lacked the ability to infer the latent variables given observed data. This limitation has been mitigated recently by methods like adversarial learned inference (ALI) [6], and related approaches. However, ALI appears to be inadequate from the standpoint of inference, in that, given observed data and associated inferred latent variables, the subsequently synthesized data often do not look particularly close to the original data.

The variational autoencoder (VAE) [13] is a class of generative models that precedes GAN. VAE learning is based on optimizing a variational lower bound, connected to inferring an approximate posterior distribution on latent variables; such learning is typically not performed in an adversarial manner. VAEs have been demonstrated to be effective models for inferring latent variables, in that the reconstructed data do typically look like the original data, albeit in a blurry manner [6]. The form of the VAE has been generalized recently, in terms of the adversarial variational Bayesian (AVB) framework [15]. This model yields general forms of encoders and decoders, but it is based on the original variational Bayesian (VB) formulation.

The original VB framework yields a lower bound on the log likelihood of the observed data, and therefore model learning is connected to maximum-likelihood (ML) approaches. From the perspective of designing generative models, it has been recognized recently that ML-based learning has limi-

tations [1]: such learning tends to yield models that match observed data, but also have a high probability of generating unrealistic synthetic data.

The original VAE employs the Kullback-Leibler divergence to constitute the variational lower bound. As is well known, the KL distance metric is asymmetric. We demonstrate that this asymmetry encourages design of decoders (generators) that often yield unrealistic synthetic data when the latent variables are drawn from the prior. From a different but related perspective, the encoder infers latent variables (across all training data) that only encompass a subset of the prior. As demonstrated below, these limitations of the encoder and decoder within conventional VAE learning are intertwined.

We consequently propose a new *symmetric* VAE (sVAE), based on a symmetric form of the KL divergence and associated variational bound. The proposed sVAE is learned using an approach related to that employed in the AVB [15], but in a new manner connected to the symmetric variational bound. Analysis of the sVAE demonstrates that it has close connections to ALI [6] and to Integral Probability Metric (IPM) [18] methods, like WGAN [2]. In fact, many adversarial learning methods, including the original GAN [9], are recovered as special cases of the proposed sVAE. This provides a new and explicit linkage between the VAE (after it is made symmetric) and a wide class of adversarially trained generative models. Additionally, with this insight, we are able to ameliorate much of the aforementioned limitations of ALI, from the perspective of data reconstruction. In addition to analyzing properties of the sVAE, we demonstrate excellent performance on an extensive set of experiments.

2 Review of Variational Autoencoder

2.1 Background

Assume observed data samples $\mathbf{x} \sim q(\mathbf{x})$, where $q(\mathbf{x})$ is the true and unknown distribution we wish to approximate. Consider $p_\theta(\mathbf{x}|\mathbf{z})$, a model with parameters θ and latent code \mathbf{z} . With prior $p(\mathbf{z})$ on the codes, the modeled generative process is $\mathbf{x} \sim p_\theta(\mathbf{x}|\mathbf{z})$, with $\mathbf{z} \sim p(\mathbf{z})$. We may marginalize out the latent codes, and hence the model is $\mathbf{x} \sim p_\theta(\mathbf{x}) = \int d\mathbf{z} p_\theta(\mathbf{x}|\mathbf{z}) p(\mathbf{z})$. To learn θ , we typically seek to maximize the expected log likelihood: $\hat{\theta} = \operatorname{argmax}_\theta \mathbb{E}_{q(\mathbf{x})} \log p_\theta(\mathbf{x})$, where one typically invokes the approximation $\mathbb{E}_{q(\mathbf{x})} \log p_\theta(\mathbf{x}) \approx \frac{1}{N} \sum_{n=1}^N \log p_\theta(\mathbf{x}_n)$ assuming N iid observed samples $\{\mathbf{x}_n\}_{n=1, N}$.

It is typically intractable to evaluate $p_\theta(\mathbf{x})$ directly, as $\int d\mathbf{z} p_\theta(\mathbf{x}|\mathbf{z}) p(\mathbf{z})$ generally doesn't have a closed form. Consequently, a typical approach is to consider a model $q_\phi(\mathbf{z}|\mathbf{x})$ for the posterior of the latent code \mathbf{z} given observed \mathbf{x} , characterized by parameters ϕ . Distribution $q_\phi(\mathbf{z}|\mathbf{x})$ is often termed an *encoder*, and $p_\theta(\mathbf{x}|\mathbf{z})$ is a *de-*

coder [13]; both are here stochastic, *vis-à-vis* their deterministic counterparts associated with a traditional autoencoder [27]. Consider the variational expression

$$\mathcal{L}_x(\theta, \phi) = \mathbb{E}_{q(\mathbf{x})} \mathbb{E}_{q_\phi(\mathbf{z}|\mathbf{x})} \log \left[\frac{p_\theta(\mathbf{x}|\mathbf{z}) p(\mathbf{z})}{q_\phi(\mathbf{z}|\mathbf{x})} \right] \quad (1)$$

In practice the expectation wrt $\mathbf{x} \sim q(\mathbf{x})$ is evaluated via sampling, assuming N observed samples $\{\mathbf{x}_n\}_{n=1, N}$. One typically must also utilize sampling from $q_\phi(\mathbf{z}|\mathbf{x})$ to evaluate the corresponding expectation in (1). Learning is effected as $(\hat{\theta}, \hat{\phi}) = \operatorname{argmax}_{\theta, \phi} \mathcal{L}_x(\theta, \phi)$, and a model so learned is termed a variational autoencoder (VAE) [13].

It is well known that $\mathcal{L}_x(\theta, \phi) = \mathbb{E}_{q(\mathbf{x})} [\log p_\theta(\mathbf{x}) - \text{KL}(q_\phi(\mathbf{z}|\mathbf{x}) \| p_\theta(\mathbf{z}|\mathbf{x}))] \leq \mathbb{E}_{q(\mathbf{x})} [\log p_\theta(\mathbf{x})]$. Alternatively, the variational expression may be represented as

$$\mathcal{L}_x(\theta, \phi) = -\text{KL}(q_\phi(\mathbf{x}, \mathbf{z}) \| p_\theta(\mathbf{x}, \mathbf{z})) + C_x \quad (2)$$

where $q_\phi(\mathbf{x}, \mathbf{z}) = q(\mathbf{x}) q_\phi(\mathbf{z}|\mathbf{x})$, $p_\theta(\mathbf{x}, \mathbf{z}) = p(\mathbf{z}) p_\theta(\mathbf{x}|\mathbf{z})$ and $C_x = \mathbb{E}_{q(\mathbf{x})} \log q(\mathbf{x})$. One may readily show that

$$\begin{aligned} & \text{KL}(q_\phi(\mathbf{x}, \mathbf{z}) \| p_\theta(\mathbf{x}, \mathbf{z})) \\ &= \mathbb{E}_{q(\mathbf{x})} \text{KL}(q_\phi(\mathbf{z}|\mathbf{x}) \| p_\theta(\mathbf{z}|\mathbf{x})) + \text{KL}(q(\mathbf{x}) \| p_\theta(\mathbf{x})) \quad (3) \\ &= \mathbb{E}_{q_\phi(\mathbf{z})} \text{KL}(q_\phi(\mathbf{x}|\mathbf{z}) \| p_\theta(\mathbf{x}|\mathbf{z})) + \text{KL}(q_\phi(\mathbf{z}) \| p(\mathbf{z})) \quad (4) \end{aligned}$$

where $q_\phi(\mathbf{z}) = \int q(\mathbf{x}) q_\phi(\mathbf{z}|\mathbf{x}) d\mathbf{x}$. To maximize $\mathcal{L}_x(\theta, \phi)$, we seek minimization of $\text{KL}(q_\phi(\mathbf{x}, \mathbf{z}) \| p_\theta(\mathbf{x}, \mathbf{z}))$. Hence, from (3) the goal is to align $p_\theta(\mathbf{x})$ with $q(\mathbf{x})$, while from (4) the goal is to align $q_\phi(\mathbf{z})$ with $p(\mathbf{z})$. The other terms seek to match the respective conditional distributions. All of these conditions are implied by minimizing $\text{KL}(q_\phi(\mathbf{x}, \mathbf{z}) \| p_\theta(\mathbf{x}, \mathbf{z}))$. However, the KL divergence is *asymmetric*, which yields limitations wrt the learned model.

2.2 Limitations of the VAE

The support $\mathcal{S}_{p(\mathbf{z})}^\epsilon$ of a distribution $p(\mathbf{z})$ is defined as the member of the set $\{\tilde{\mathcal{S}}_{p(\mathbf{z})}^\epsilon : \int_{\tilde{\mathcal{S}}_{p(\mathbf{z})}^\epsilon} p(\mathbf{z}) d\mathbf{z} = 1 - \epsilon\}$ with minimum size $\|\tilde{\mathcal{S}}_{p(\mathbf{z})}^\epsilon\| \triangleq \int_{\tilde{\mathcal{S}}_{p(\mathbf{z})}^\epsilon} d\mathbf{z}$. We are typically interested in $\epsilon \rightarrow 0^+$. For notational convenience we replace $\mathcal{S}_{p(\mathbf{z})}^\epsilon$ with $\mathcal{S}_{p(\mathbf{z})}$, with the understanding ϵ is small. We also define $\mathcal{S}_{p(\mathbf{z})_-}$ as the largest set for which $\int_{\mathcal{S}_{p(\mathbf{z})_-}} p(\mathbf{z}) d\mathbf{z} = \epsilon$, and hence $\int_{\mathcal{S}_{p(\mathbf{z})}} p(\mathbf{z}) d\mathbf{z} + \int_{\mathcal{S}_{p(\mathbf{z})_-}} p(\mathbf{z}) d\mathbf{z} = 1$. For simplicity of exposition, we assume $\mathcal{S}_{p(\mathbf{z})}$ and $\mathcal{S}_{p(\mathbf{z})_-}$ are unique; the meaning of the subsequent analysis is unaffected by this assumption.

Consider $-\text{KL}(q(\mathbf{x}) \| p_\theta(\mathbf{x})) = \mathbb{E}_{q(\mathbf{x})} \log p_\theta(\mathbf{x}) - C_x$, which from (2) and (3) we seek to make large when learning θ . The following discussion borrows insights from [2], although that analysis was different, in that it was not placed within the context of the VAE. Since $\int_{\mathcal{S}_{q(\mathbf{x})_-}} q(\mathbf{x}) \log p_\theta(\mathbf{x}) d\mathbf{x} \approx 0$,

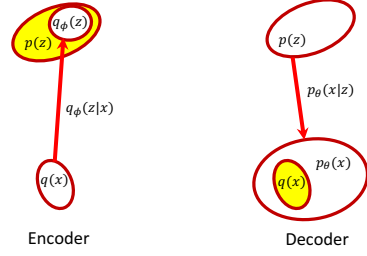


Figure 1: Characteristics of the encoder and decoder of the conventional VAE \mathcal{L}_x , for which the support of the distributions satisfy $\mathcal{S}_{q(x)} \subset \mathcal{S}_{p_\theta(x)}$ and $\mathcal{S}_{q_\phi(z)} \subset \mathcal{S}_{p(z)}$, implying that the generative model $p_\theta(x)$ has a high probability of generating unrealistic draws.

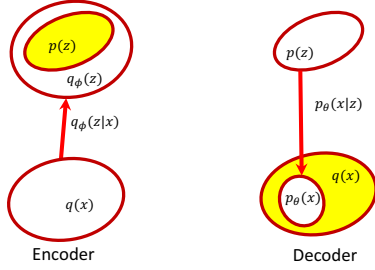


Figure 2: Characteristics of the new VAE expression, \mathcal{L}_z .

$\mathbb{E}_{q(x)} \log p_\theta(x) \approx \int_{\mathcal{S}_{q(x)}} q(x) \log p_\theta(x) dx$, and $\mathcal{S}_{q(x)} = (\mathcal{S}_{q(x)} \cap \mathcal{S}_{p_\theta(x)}) \cup (\mathcal{S}_{q(x)} \cap \mathcal{S}_{p_\theta(x)_-})$. If $\mathcal{S}_{q(x)} \cap \mathcal{S}_{p_\theta(x)_-} \neq \emptyset$, there is a strong (negative) penalty introduced by $\int_{\mathcal{S}_{q(x)} \cap \mathcal{S}_{p_\theta(x)_-}} q(x) \log p_\theta(x) dx$, and therefore maximization of $\mathbb{E}_{q(x)} \log p_\theta(x)$ encourages $\mathcal{S}_{q(x)} \cap \mathcal{S}_{p_\theta(x)_-} = \emptyset$. By contrast, there is not a substantial penalty to $\mathcal{S}_{q(x)_-} \cap \mathcal{S}_{p_\theta(x)} \neq \emptyset$.

Summarizing these conditions, the goal of maximizing $-\text{KL}(q(x)||p_\theta(x))$ encourages $\mathcal{S}_{q(x)} \subset \mathcal{S}_{p_\theta(x)}$. This implies that $p_\theta(x)$ can synthesize all x that may be drawn from $q(x)$, but additionally there is (often) high probability that $p_\theta(x)$ will synthesize x that will *not* be drawn from $q(x)$.

Similarly, $-\text{KL}(q_\phi(z)||p(z)) = h(q_\phi(z)) + \mathbb{E}_{q_\phi(z)} \log p(z)$ encourages $\mathcal{S}_{q_\phi(z)} \subset \mathcal{S}_{p(z)}$, and the commensurate goal of increasing differential entropy $h(q_\phi(z)) = -\mathbb{E}_{q_\phi(z)} \log q_\phi(z)$ encourages that $\mathcal{S}_{q_\phi(z)} \cap \mathcal{S}_{p(z)}$ be as large as possible.

Hence, the goal of large $-\text{KL}(q(x)||p_\theta(x))$ and $-\text{KL}(q_\phi(z)||p(z))$ are saying the same thing, from different perspectives: (i) seeking large $-\text{KL}(q(x)||p_\theta(x))$ implies that there is a high probability that x drawn from $p_\theta(x)$ will be different from those drawn from $q(x)$, and (ii) large $-\text{KL}(q_\phi(z)||p(z))$ implies that z drawn from $p(z)$ are likely to be different from those drawn from $q_\phi(z)$, with $z \in \{\mathcal{S}_{p(z)} \cap \mathcal{S}_{q_\phi(z)_-}\}$ responsible for the x that are inconsistent with $q(x)$. These properties are summarized in Fig. 1.

Considering the remaining terms in (3) and (4), and using similar logic on $-\mathbb{E}_{q(x)} \text{KL}(q_\phi(z|x)||p_\theta(z|x)) = h(q_\phi(z|x)) + \mathbb{E}_{q(x)} \mathbb{E}_{q_\phi(z|x)} \log p_\theta(z|x)$, the model encourages $\mathcal{S}_{q_\phi(z|x)} \subset \mathcal{S}_{p_\theta(z|x)}$. From $-\mathbb{E}_{q_\phi(z)} \text{KL}(q_\phi(x|z)||p_\theta(x|z)) = h(q_\phi(x|z)) + \mathbb{E}_{q_\phi(z)} \mathbb{E}_{q_\phi(x|z)} \log p_\theta(x|z)$, the model also encourages $\mathcal{S}_{q_\phi(x|z)} \subset \mathcal{S}_{p_\theta(x|z)}$. The differential entropies $h(q_\phi(z|x))$ and $h(q_\phi(x|z))$ encourage that $\mathcal{S}_{q_\phi(z|x)} \cap \mathcal{S}_{p_\theta(z|x)}$ and $\mathcal{S}_{q_\phi(x|z)} \cap \mathcal{S}_{p_\theta(x|z)}$ be as large as possible. Since $\mathcal{S}_{q_\phi(z|x)} \subset \mathcal{S}_{p_\theta(z|x)}$, it is anticipated that $q_\phi(z|x)$ will under-estimate the variance of $p_\theta(x|z)$, as is common with the variational approximation to the posterior [4].

3 Refined VAE: Imposition of Symmetry

3.1 Symmetric KL divergence

Consider the new variational expression

$$\begin{aligned} \mathcal{L}_z(\theta, \phi) &= \mathbb{E}_{p(z)} \mathbb{E}_{p_\theta(x|z)} \log \left[\frac{q_\phi(z|x)q(x)}{p_\theta(x|z)} \right] \quad (5) \\ &= -\text{KL}(p_\theta(x, z)||q_\phi(x, z)) + C_z \quad (6) \end{aligned}$$

where $C_z = -h(p(z))$. Using logic analogous to that applied to \mathcal{L}_x , maximization of \mathcal{L}_z encourages distribution supports reflected in Fig. 2.

Defining $\mathcal{L}_{xz}(\theta, \phi) = \mathcal{L}_x(\theta, \phi) + \mathcal{L}_z(\theta, \phi)$, we have

$$\mathcal{L}_{xz}(\theta, \phi) = -\text{KL}_s(q_\phi(x, z)||p_\theta(x, z)) + K \quad (7)$$

where $K = C_x + C_z$, and the *symmetric* KL divergence is $\text{KL}_s(q_\phi(x, z)||p_\theta(x, z)) \triangleq \text{KL}(q_\phi(x, z)||p_\theta(x, z)) + \text{KL}(p_\theta(x, z)||q_\phi(x, z))$. Maximization of $\mathcal{L}_{xz}(\theta, \phi)$ seeks minimizing $\text{KL}_s(q_\phi(x, z)||p_\theta(x, z))$, which *simultaneously* imposes the conditions summarized in Figs. 1 and 2.

One may show that

$$\begin{aligned} \text{KL}_s(q_\phi(x, z)||p_\theta(x, z)) &= \mathbb{E}_{p(z)} \text{KL}(p_\theta(x|z)||q_\phi(x|z)) \\ &\quad + \mathbb{E}_{q_\phi(z)} \text{KL}(q_\phi(x|z)||p_\theta(x|z)) + \text{KL}_s(p(z)||q_\phi(z)) \quad (8) \\ &= \mathbb{E}_{p_\theta(x)} \text{KL}(p_\theta(z|x)||q_\phi(z|x)) \\ &\quad + \mathbb{E}_{q_\phi(x)} \text{KL}(q_\phi(z|x)||p_\theta(z|x)) + \text{KL}_s(p_\theta(x)||q(x)) \quad (9) \end{aligned}$$

Considering the representation in (9), the goal of small $\text{KL}_s(p_\theta(x)||q(x))$ encourages $\mathcal{S}_{q(x)} \subset \mathcal{S}_{p_\theta(x)}$ and $\mathcal{S}_{p_\theta(x)} \subset \mathcal{S}_{q(x)}$, and hence that $\mathcal{S}_{q(x)} = \mathcal{S}_{p_\theta(x)}$. Further, since $-\text{KL}_s(p_\theta(x)||q(x)) = \mathbb{E}_{q(x)} \log p_\theta(x) + \mathbb{E}_{p_\theta(x)} \log q(x) + h(p_\theta(x)) - C_x$, maximization of $-\text{KL}_s(p_\theta(x)||q(x))$ seeks to minimize the cross-entropy between $q(x)$ and $p_\theta(x)$, encouraging a complete matching of the distributions $q(x)$ and $p_\theta(x)$, not just shared support. From (8), a match is simultaneously encouraged between $p(z)$ and $q_\phi(z)$. Further, the respective conditional distributions are also encouraged to match.

3.2 Adversarial solution

Assuming fixed (θ, ϕ) , and using logic analogous to Proposition 1 in [15], we consider

$$\begin{aligned} g(\psi) &= \mathbb{E}_{q_\phi(\mathbf{x}, \mathbf{z})} \log(1 - \sigma(f_\psi(\mathbf{x}, \mathbf{z}))) \\ &+ \mathbb{E}_{p_\theta(\mathbf{x}, \mathbf{z})} \log \sigma(f_\psi(\mathbf{x}, \mathbf{z})) \end{aligned} \quad (10)$$

where $\sigma(\zeta) = 1/(1 + \exp(-\zeta))$. The scalar function $f_\psi(\mathbf{x}, \mathbf{z})$ is represented by a deep neural network with parameters ψ , and network inputs (\mathbf{x}, \mathbf{z}) . For fixed (θ, ϕ) , the parameters ψ^* that maximize $g(\psi)$ yield

$$f_{\psi^*}(\mathbf{x}, \mathbf{z}) = \log p_\theta(\mathbf{x}, \mathbf{z}) - \log q_\phi(\mathbf{x}, \mathbf{z}) \quad (11)$$

and hence

$$\mathcal{L}_x(\theta, \phi) = \mathbb{E}_{q_\phi(\mathbf{x}, \mathbf{z})} f_{\psi^*}(\mathbf{x}, \mathbf{z}) + C_x \quad (12)$$

$$\mathcal{L}_z(\theta, \phi) = -\mathbb{E}_{p_\theta(\mathbf{x}, \mathbf{z})} f_{\psi^*}(\mathbf{x}, \mathbf{z}) + C_z \quad (13)$$

Hence, to optimize $\mathcal{L}_{xz}(\theta, \phi)$ we consider the cost function

$$\begin{aligned} \ell(\theta, \phi; \psi^*) &= \mathbb{E}_{q_\phi(\mathbf{x}, \mathbf{z})} f_{\psi^*}(\mathbf{x}, \mathbf{z}) \\ &- \mathbb{E}_{p_\theta(\mathbf{x}, \mathbf{z})} f_{\psi^*}(\mathbf{x}, \mathbf{z}) \end{aligned} \quad (14)$$

Assuming (11) holds, we have

$$\ell(\theta, \phi; \psi^*) = -\text{KL}_s(q_\phi(\mathbf{x}, \mathbf{z}) \| p_\theta(\mathbf{x}, \mathbf{z})) \leq 0 \quad (15)$$

and the goal is to achieve $\ell(\theta, \phi; \psi^*) = 0$ through joint optimization of $(\theta, \phi; \psi^*)$. Model learning consists of alternating between (10) and (14), maximizing (10) wrt ψ with (θ, ϕ) fixed, and maximizing (14) wrt (θ, ϕ) with ψ fixed.

The expectations in (10) and (14) are approximated by averaging over samples, and therefore to implement this solution we need only be able to sample from $p_\theta(\mathbf{x}|\mathbf{z})$ and $q_\phi(\mathbf{z}|\mathbf{x})$, and we do not require explicit forms for these distributions. For example, a draw from $q_\phi(\mathbf{z}|\mathbf{x})$ may be constituted as $\mathbf{z} = h_\phi(\mathbf{x}, \epsilon)$, where $h_\phi(\mathbf{x}, \epsilon)$ is implemented as a neural network with parameters ϕ and $\epsilon \sim \mathcal{N}(\mathbf{0}, \mathbf{I})$.

3.3 Interpretation in terms of LRT statistic

In (10) a classifier is designed to distinguish between samples (\mathbf{x}, \mathbf{z}) drawn from $p_\theta(\mathbf{x}, \mathbf{z}) = p(\mathbf{z})p_\theta(\mathbf{x}|\mathbf{z})$ and from $q_\phi(\mathbf{x}, \mathbf{z}) = q(\mathbf{x})q_\phi(\mathbf{z}|\mathbf{x})$. Implicit in that expression is that there is equal probability that either of these distributions are selected for drawing (\mathbf{x}, \mathbf{z}) , i.e., that $(\mathbf{x}, \mathbf{z}) \sim [p_\theta(\mathbf{x}, \mathbf{z}) + q_\phi(\mathbf{x}, \mathbf{z})]/2$. Under this assumption, given observed (\mathbf{x}, \mathbf{z}) , the probability of it being drawn from $p_\theta(\mathbf{x}, \mathbf{z})$ is $p_\theta(\mathbf{x}, \mathbf{z})/(p_\theta(\mathbf{x}, \mathbf{z}) + q_\phi(\mathbf{x}, \mathbf{z}))$, and the probability of it being drawn from $q_\phi(\mathbf{x}, \mathbf{z})$ is $q_\phi(\mathbf{x}, \mathbf{z})/(p_\theta(\mathbf{x}, \mathbf{z}) + q_\phi(\mathbf{x}, \mathbf{z}))$ [9]. Since the denominator

$p_\theta(\mathbf{x}, \mathbf{z}) + q_\phi(\mathbf{x}, \mathbf{z})$ is shared by these distributions, and assuming function $p_\theta(\mathbf{x}, \mathbf{z})/q_\phi(\mathbf{x}, \mathbf{z})$ is known, an observed (\mathbf{x}, \mathbf{z}) is inferred as being drawn from the underlying distributions as

$$\text{if } p_\theta(\mathbf{x}, \mathbf{z})/q_\phi(\mathbf{x}, \mathbf{z}) > 1, \quad (\mathbf{x}, \mathbf{z}) \rightarrow p_\theta(\mathbf{x}, \mathbf{z}) \quad (16)$$

$$\text{if } p_\theta(\mathbf{x}, \mathbf{z})/q_\phi(\mathbf{x}, \mathbf{z}) < 1, \quad (\mathbf{x}, \mathbf{z}) \rightarrow q_\phi(\mathbf{x}, \mathbf{z}) \quad (17)$$

This is the well-known likelihood ratio test (LRT) [26], and is reflected by (11). We have therefore derived a learning procedure based on the log-LRT, as reflected in (14). The solution is ‘‘adversarial,’’ in the sense that when optimizing (θ, ϕ) the objective in (14) seeks to ‘‘fool’’ the LRT test statistic, while for fixed (θ, ϕ) maximization of (10) wrt ψ corresponds to updating the LRT. This adversarial solution comes as a natural consequence of symmetrizing the traditional VAE learning procedure.

4 Connections to Prior Work

The adversarially learned inference (ALI) [6] framework seeks to learn both an encoder and decoder, like the approach proposed above, and is based on optimizing

$$\begin{aligned} (\hat{\theta}, \hat{\phi}) &= \underset{\theta, \phi}{\text{argmin}} \max_{\psi} \{ \mathbb{E}_{p_\theta(\mathbf{x}, \mathbf{z})} \log \sigma(f_\psi(\mathbf{x}, \mathbf{z})) \\ &+ \mathbb{E}_{q_\phi(\mathbf{x}, \mathbf{z})} \log(1 - \sigma(f_\psi(\mathbf{x}, \mathbf{z}))) \} \end{aligned} \quad (18)$$

This has similarities to the proposed approach, in that the term $\max_{\psi} \mathbb{E}_{p_\theta(\mathbf{x}, \mathbf{z})} \log \sigma(f_\psi(\mathbf{x}, \mathbf{z})) + \mathbb{E}_{q_\phi(\mathbf{x}, \mathbf{z})} \log(1 - \sigma(f_\psi(\mathbf{x}, \mathbf{z})))$ is identical to our maximization of (10) wrt ψ . However, in the proposed approach, rather than directly then optimizing wrt (θ, ϕ) , as in (18), in (14) the result from this term is used to define $f_{\psi^*}(\mathbf{x}, \mathbf{z})$, which is then employed in (14) to subsequently optimize over (θ, ϕ) .

Note that $\log \sigma(\cdot)$ is a monotonically increasing function, and therefore we may replace (14) as

$$\begin{aligned} \ell'(\theta, \phi; \psi^*) &= \mathbb{E}_{q_\phi(\mathbf{x}, \mathbf{z})} \log \sigma(f_{\psi^*}(\mathbf{x}, \mathbf{z})) \\ &+ \mathbb{E}_{p_\theta(\mathbf{x}, \mathbf{z})} \log \sigma(-f_{\psi^*}(\mathbf{x}, \mathbf{z})) \end{aligned} \quad (19)$$

and note $\sigma(-f_{\psi^*}(\mathbf{x}, \mathbf{z}; \theta, \phi)) = 1 - \sigma(f_{\psi^*}(\mathbf{x}, \mathbf{z}; \theta, \phi))$. Maximizing (19) wrt (θ, ϕ) with fixed ψ^* corresponds to the minimization wrt (θ, ϕ) reflected in (18). Hence, the proposed approach is *exactly* ALI, if in (14) we replace $\pm f_{\psi^*}$ with $\log \sigma(\pm f_{\psi^*})$.

The proposed approach assumed both a decoder $p_\theta(\mathbf{x}|\mathbf{z})$ and an encoder $q_\phi(\mathbf{z}|\mathbf{x})$, and we considered the symmetric $\text{KL}_s(q_\phi(\mathbf{x}, \mathbf{z}) \| p_\theta(\mathbf{x}, \mathbf{z}))$. We now simplify the model for the case in which we only have a decoder, and the synthesized data are drawn $\mathbf{x} \sim p_\theta(\mathbf{x}|\mathbf{z})$ with $\mathbf{z} \sim p(\mathbf{z})$, and we wish to learn θ such that data synthesized in this manner match observed data $\mathbf{x} \sim q(\mathbf{x})$. Consider the symmetric

$$\begin{aligned} \text{KL}_s(q(\mathbf{x}) \| p_\theta(\mathbf{x})) &= \mathbb{E}_{p(\mathbf{z})} \mathbb{E}_{p_\theta(\mathbf{x}|\mathbf{z})} f_{\psi^*}(\mathbf{x}) \\ &- \mathbb{E}_{q(\mathbf{x})} f_{\psi^*}(\mathbf{x}) \end{aligned} \quad (20)$$

where for fixed θ

$$f_{\psi^*}(\mathbf{x}) = \log(p_{\theta}(\mathbf{x})/q(\mathbf{x})) \quad (21)$$

We consider a simplified form of (10), specifically

$$g(\psi) = \mathbb{E}_{p(\mathbf{z})} \mathbb{E}_{p_{\theta}(\mathbf{x}|\mathbf{z})} \log \sigma(f_{\psi}(\mathbf{x})) + \mathbb{E}_{q(\mathbf{x})} \log(1 - \sigma(f_{\psi}(\mathbf{x}))) \quad (22)$$

which we seek to maximize wrt ψ with fixed θ , with optimal solution as in (21). We optimize θ seeking to maximize $-\text{KL}_s(q(\mathbf{x})\|p_{\theta}(\mathbf{x}))$, as $\text{argmax}_{\theta} \ell(\theta; \psi^*)$ where

$$\ell(\theta; \psi^*) = \mathbb{E}_{q(\mathbf{x})} f_{\psi^*}(\mathbf{x}) - \mathbb{E}_{p_{\theta}(\mathbf{x}, \mathbf{z})} f_{\psi^*}(\mathbf{x}) \quad (23)$$

where $\mathbb{E}_{q(\mathbf{x})} f_{\psi^*}(\mathbf{x})$ is independent of the update parameter θ . We observe that in seeking to maximize $\ell(\theta; \psi^*)$, parameters θ are updated as to “fool” the log-LRT $\log[q(\mathbf{x})/p_{\theta}(\mathbf{x})]$. Learning consists of iteratively updating ψ by maximizing $g(\psi)$ and updating θ by maximizing $\ell(\theta; \psi^*)$.

Recall that $\log \sigma(\cdot)$ is a monotonically increasing function, and therefore we may replace (23) as

$$\ell'(\theta; \psi^*) = \mathbb{E}_{p_{\theta}(\mathbf{x}, \mathbf{z})} \log \sigma(-f_{\psi^*}(\mathbf{x})) \quad (24)$$

Using the same logic as discussed above in the context of ALI, maximizing $\ell'(\theta; \psi^*)$ wrt θ may be replaced by minimization, by transforming $\sigma(\mu) \rightarrow \sigma(-\mu)$. With this simple modification, minimizing the modified (24) wrt θ and maximizing (22) wrt ψ , we *exactly* recover the original GAN [9], for the special (but common) case of a sigmoidal discriminator.

The Integral Probability Metric (IPM) [18] setup is represented as

$$\hat{\theta} = \underset{\psi}{\text{argmin}}_{\theta} \max_{\psi} \{ \mathbb{E}_{q(\mathbf{x})} f_{\psi}(\mathbf{x}) - \mathbb{E}_{p_{\theta}(\mathbf{x}, \mathbf{z})} f_{\psi}(\mathbf{x}) \} \quad (25)$$

Different classes of functions $f_{\psi}(\mathbf{x})$ yield different learning metrics, including energy-based GAN [28], Maximum Mean Discrepancy [10], Fisher GAN [16], Wasserstein GAN (WGAN) [2], McGAN [17], among many other possible forms.

In WGAN, for example, $f_{\psi}(\mathbf{x})$ must be a 1-Lipschitz function. Typically $f_{\psi}(\mathbf{x})$ is represented by a neural network with parameters ψ , with parameter clipping or ℓ_2 regularization on the weights (to constrain the amplitude of $f_{\psi}(\mathbf{x})$). Note that WGAN is closely related to (23), but in WGAN $f_{\psi}(\mathbf{x})$ doesn’t make an explicit connection to the underlying likelihood ratio, as in (21).

It is believed that the current paper is the first to consider symmetric variational learning, introducing \mathcal{L}_z , from which we have made explicit connections to previously

developed adversarial-learning methods. Previous efforts have been made to match $q_{\phi}(\mathbf{z})$ to $p(\mathbf{z})$, which is a consequence of the proposed symmetric VAE (sVAE). For example, [14] introduced a modification to the original VAE formulation, but it loses connection to the variational lower bound [15].

5 Model Augmentation

A significant limitation of the original ALI setup is an inability to accurately reconstruct observed data via the process $\mathbf{x} \rightarrow \mathbf{z} \rightarrow \hat{\mathbf{x}}$ [6]. With the proposed sVAE, which is intimately connected to ALI, we may readily address this shortcoming. The variational expressions discussed above may be written as $\mathcal{L}_x = \mathbb{E}_{q_{\phi}(\mathbf{x}, \mathbf{z})} \log p_{\theta}(\mathbf{x}|\mathbf{z}) - \mathbb{E}_{q(\mathbf{x})} \text{KL}(q_{\phi}(\mathbf{z}|\mathbf{x})\|p(\mathbf{z}))$ and $\mathcal{L}_z = \mathbb{E}_{p_{\theta}(\mathbf{x}, \mathbf{z})} \log q_{\phi}(\mathbf{z}|\mathbf{x}) - \mathbb{E}_{p(\mathbf{z})} \text{KL}(p_{\theta}(\mathbf{x}|\mathbf{z})\|q(\mathbf{x}))$. In both of these expressions, the first term to the right of the equality enforces model fit, and the second term penalizes the posterior distribution for *individual data samples* for being dissimilar from the prior (i.e., penalizes $q_{\phi}(\mathbf{z}|\mathbf{x})$ from being dissimilar from $p(\mathbf{z})$, and likewise wrt $p_{\theta}(\mathbf{x}|\mathbf{z})$ and $q(\mathbf{x})$). The proposed sVAE encourages the *cumulative* distributions $q_{\phi}(\mathbf{z})$ and $p_{\theta}(\mathbf{x})$ to match $p(\mathbf{z})$ and $q(\mathbf{x})$, respectively; by simultaneously encouraging more peaked $q_{\phi}(\mathbf{z}|\mathbf{x})$ and $p_{\theta}(\mathbf{x}|\mathbf{z})$, we anticipate better “cycle consistency” [30] and hence more accurate reconstructions.

To encourage $q_{\phi}(\mathbf{z}|\mathbf{x})$ that are more peaked in the space of \mathbf{z} for individual \mathbf{x} , and also to consider more peaked $p_{\theta}(\mathbf{x}|\mathbf{z})$, we may augment the variational expressions as

$$\mathcal{L}'_x = (\lambda + 1) \mathbb{E}_{q_{\phi}(\mathbf{x}, \mathbf{z})} \log p_{\theta}(\mathbf{x}|\mathbf{z}) - \mathbb{E}_{q(\mathbf{x})} \text{KL}(q_{\phi}(\mathbf{z}|\mathbf{x})\|p(\mathbf{z})) \quad (26)$$

$$\mathcal{L}'_z = (\lambda + 1) \mathbb{E}_{p_{\theta}(\mathbf{x}, \mathbf{z})} \log q_{\phi}(\mathbf{z}|\mathbf{x}) - \mathbb{E}_{p(\mathbf{z})} \text{KL}(p_{\theta}(\mathbf{x}|\mathbf{z})\|q(\mathbf{x})) \quad (27)$$

where $\lambda \geq 0$. For $\lambda = 0$ the original variational expressions are retained, and for $\lambda > 0$, $q_{\phi}(\mathbf{z}|\mathbf{x})$ and $p_{\theta}(\mathbf{x}|\mathbf{z})$ are allowed to diverge more from $p(\mathbf{z})$ and $q(\mathbf{x})$, respectively, while placing more emphasis on the data-fit terms. Defining $\mathcal{L}'_{xz} = \mathcal{L}'_x + \mathcal{L}'_z$, we have

$$\mathcal{L}'_{xz} = \mathcal{L}_{xz} + \lambda [\mathbb{E}_{q_{\phi}(\mathbf{x}, \mathbf{z})} \log p_{\theta}(\mathbf{x}|\mathbf{z}) + \mathbb{E}_{p_{\theta}(\mathbf{x}, \mathbf{z})} \log q_{\phi}(\mathbf{z}|\mathbf{x})] \quad (28)$$

Model learning is the same as discussed in Sec. 3.2, with the modification

$$\ell'(\theta, \phi; \psi^*) = \mathbb{E}_{q_{\phi}(\mathbf{x}, \mathbf{z})} [f_{\psi^*}(\mathbf{x}, \mathbf{z}) + \lambda \log p_{\theta}(\mathbf{x}|\mathbf{z})] - \mathbb{E}_{p_{\theta}(\mathbf{x}, \mathbf{z})} [f_{\psi^*}(\mathbf{x}, \mathbf{z}) - \lambda \log q_{\phi}(\mathbf{z}|\mathbf{x})] \quad (29)$$

A disadvantage of this approach is that it requires explicit forms for $p_{\theta}(\mathbf{x}|\mathbf{z})$ and $q_{\phi}(\mathbf{z}|\mathbf{x})$, while the setup in Sec. 3.2 only requires the ability to sample from these distributions. We have found that, when employing explicit forms

Table 1: Quantitative Results on MNIST

Model	NLL	IS
NF (k=80) [21]	85.1	-
PixelRNN [19]	79.2	-
GAN [9]	-	$8.34 \pm .03$
WGAN-GP [11]	-	$8.45 \pm .04$
sVAE	81.14	$9.15 \pm .06$
sVAE-r	82.51	$9.29 \pm .06$

for $p_{\theta}(\mathbf{x}|\mathbf{z})$ and $q_{\phi}(\mathbf{z}|\mathbf{x})$, simple Gaussian models work well, with associated means and variances manifested via a deep neural network (see the Appendix for detailed descriptions of the employed deep networks).

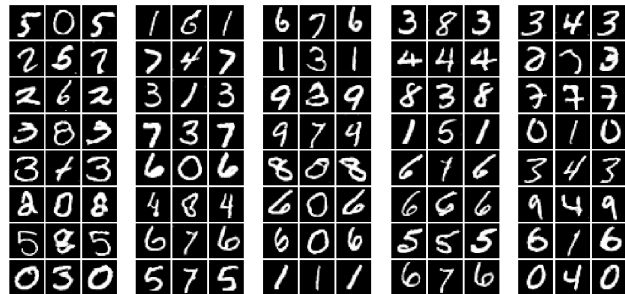
6 Experiments

We consider the MNIST, CIFAR-10 and ImageNet datasets, for both reconstruction and generation tasks. The quantitative evaluation for reconstruction quality is based on the negative log-likelihood (NLL) estimated via the variational lower bound defined in (1), while generation quality is based on inception score (IS) [22]. For the first two datasets, we show results based on two models: *i*) sVAE: the model developed in Sec. 3 to optimize $g(\psi)$ in (10) and $\ell(\theta, \phi; \psi^*)$ in (14); *ii*) sVAE-r: sVAE with reconstruction loss discussed in Sec. 5 to optimize $g(\psi)$ in (10) and $\ell'(\theta, \phi; \psi^*)$ in (29). For the ImageNet dataset, we only show results based on sVAE-r.

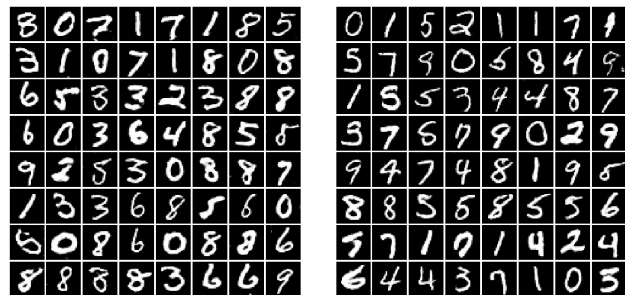
All parameters are initialized with Xavier [8] and optimized using Adam [12] with learning rate of 0.0001. λ is set to 0.3 for all datasets when considering sVAE-r. No dataset-specific tuning or regularization other than dropout [24] is performed. The architectures for the encoder $q_{\phi}(\mathbf{z}|\mathbf{x})$, decoder $p_{\theta}(\mathbf{x}|\mathbf{z})$, and discriminator $f_{\psi}(\mathbf{x}, \mathbf{z})$ are detailed in the Appendix.

6.1 MNIST

Considering the MNIST dataset, the results of image generation and reconstruction for sVAE and sVAE-r are shown in Figure 3. In addition, quantitative results are summarized in Table 1 using inception score (IS) and negative log-likelihood (NLL). By adding the reconstruction loss, sVAE-r overcomes the limitation of image reconstruction in ALI [6]. It achieves a negative log-likelihood of 81.14 nats, outperforming normalizing flow (85.1 nats) with a similar architecture, while also being competitive to the state-of-the-art (79.2 nats). Meanwhile, both sVAE and sVAE-r are able to provide compelling generated images, outperforming GAN [9] and WGAN-GP [11] based on the inception scores.



(a)



(b)

Figure 3: sVAE and sVAE-r results on MNIST. (a) Reconstructed images. In each block: column one for ground-truth, column two for sVAE and column three for sVAE-r. (b) Generated sample images by sVAE.

Table 2: Quantitative Results on CIFAR-10; \dagger 2.96 is based on our implementation and 2.92 is reported in [23].

Method	NLL(bits)	RMSE	IS
WGAN [3]	-	-	3.82
MIX+WassersteinGAN [3]	-	-	4.05
DCGAN [20]	-	-	4.89
ALI [6]	-	14.53	4.79
PixelRNN [19]	3.06	-	-
PixelCNN++ [23]	2.96 (2.92) \dagger	3.289	5.51
sVAE-r	3.09	3.17	6.96
sVAE	3.32	3.36	6.76

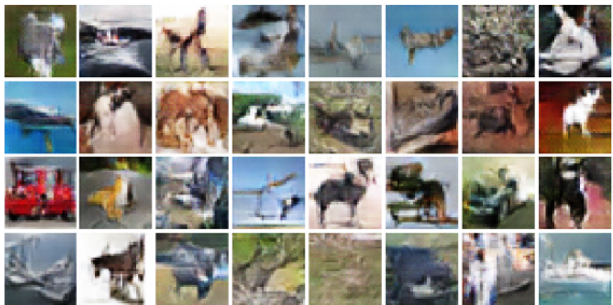
6.2 CIFAR

Considering the CIFAR-10 dataset, quantitative results are summarized in Table 2. Compared with state-of-the-art ML-based models [23, 19], our model gives competitive results on reconstruction. Note that our negative evidence lower bound (ELBO) is an upper bound of NLL as reported in [23, 19]. Moreover, sVAE also provides much better performance on generation based on IS, outperforming other adversarially-trained models. The generated samples are shown in Figure 4.

ALI [6], which also seeks to match the joint encoder and decoder distribution, is also implemented as a baseline. Since the decoder in ALI is a deterministic network, the NLL of ALI is impractical to compute. Alternatively, we report the root-mean-square-error (RMSE) of reconstruc-



(a)



(b)

Figure 4: Samples generated by sVAE (a) and sVAE-r (b) when trained on CIFAR-10.



Figure 5: Comparison of sVAE-r with ALI [6]. In each block: column one for ground-truth, column two for ALI and column three for sVAE-r.

tion as a reference. Figure 5 qualitatively compares the reconstruction performance of ALI and sVAE-r. As can be seen, the reconstruction of ALI is related to but not a faithful reproduction of the input data, which evidences the limitation in reconstruction ability of adversarial learning. This is also consistent based on RMSE, in which sVAE-r achieves a smaller score than ALI.

Table 3: Quantitative Results on ImageNet.

Method	NLL	IS
DCGAN [20]	-	5.965
PixelRNN [19]	3.63	-
PixelCNN++ [23]	3.27	7.65
sVAE-r	3.71	11.14

6.3 ImageNet

To evaluate the scalability of our model to large datasets, we use ImageNet 2012 with images resized to 64×64 . We only show the results for sVAE-r since it outperforms sVAE on both generation and reconstruction tasks on MNIST and CIFAR-10. The quantitative results in Table 3 show that sVAE-r significantly improves the performance on generation compared with DCGAN and PixelCNN++, while achieving competitive results on reconstruction compared with PixelRNN and PixelCNN++.

Note that PixelCNN++ takes more than two weeks (44 hours per epoch) for training and 52.0 seconds/image for generating samples, while our model only requires less than 2 days (4 hours per epoch) for training and 0.01 seconds/image for generating on a single TITAN X GPU. As a reference, the true validation set of ImageNet 2012 achieves 53.24% accuracy. This is because ImageNet has much greater variety of images than CIFAR-10. Figure 6 shows generated samples of ImageNet by sVAE-r, compared with DCGAN and PixelCNN++. As can be seen, our model is able to produce sharp images, without using label information, while capturing more local spatial dependencies than PixelCNN++. In addition, it does not suffer from mode collapse like DCGAN.

7 Conclusions

We present the symmetric variational autoencoder (sVAE), a novel framework that matches the joint distribution of data and its associated latent code using the *symmetric* Kullback-Leibler divergence. The experiment results demonstrate that sVAE overcomes the missing-mode problem, and our experience is that it is very stable to train. The sVAE yields as special cases many prior adversarial methods, and it does so within a principled generalization of variational learning. Excellent performance is demonstrated for image generation and reconstruction, and sVAE is well matched to semi-supervised learning tasks, which we will address in future work.

References

[1] M. Arjovsky and L. Bottou. Towards principled methods for training generative adversarial networks. In *ICLR*, 2017.

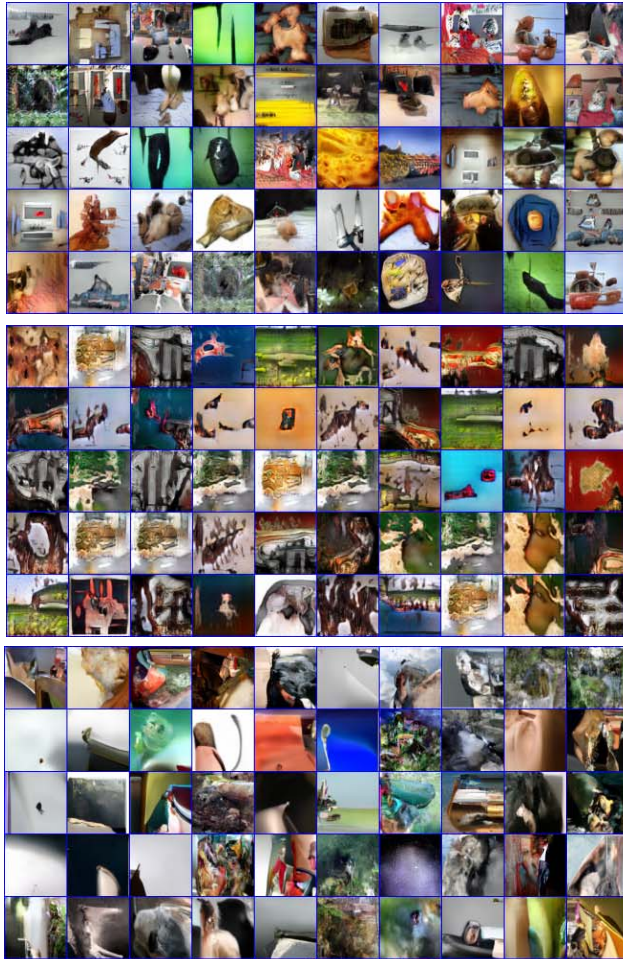


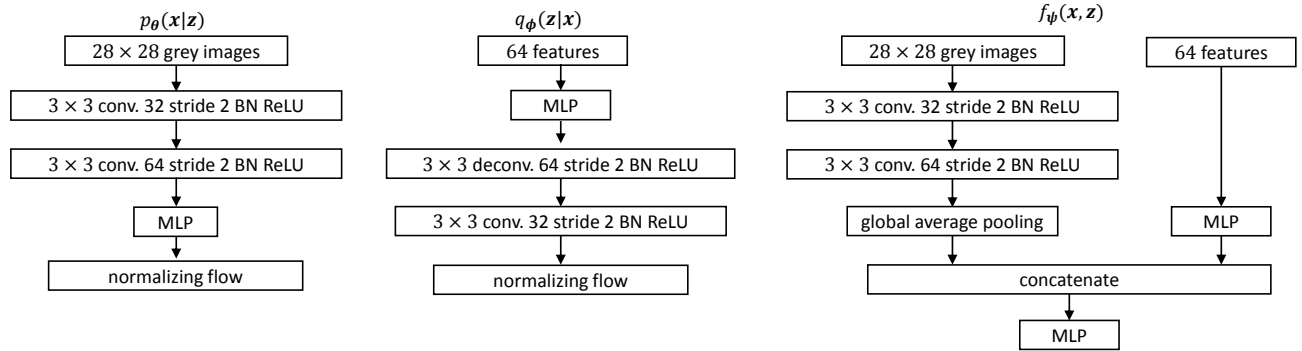
Figure 6: Generated samples trained on ImageNet. (Top) sVAE-r; (Middle) DCGAN [20];(Bottom) PixelCNN++ [23].

- [2] M. Arjovsky, S. Chintala, and L. Bottou. Wasserstein GAN. In *ICLR*, 2017.
- [3] S. Arora, R. Ge, Y. Liang, T. Ma, and Y. Zhang. Generalization and equilibrium in generative adversarial nets. In *arXiv*, 2017.
- [4] D.M. Blei, A. Kucukelbir, and J.D. McAuliffe. Variational inference: A review for statisticians. In *arXiv:1601.00670v5*, 2017.
- [5] J.E. Lucas J.R. Nevins Q. Wang C.M. Carvalho, J. Chang and M. West. High-dimensional sparse factor modeling: Applications in gene expression genomics. *JASA*, 2008.
- [6] V. Dumoulin, I. Belghazi, B. Poole, A. Lamb, O. Mastropietro, and A. Courville. Adversarially learned inference. In *ICLR*, 2017.
- [7] Z. Ghahramani and G.E. Hinton. The em algorithm for mixtures of factor analyzers. Technical report, University of Toronto, 1997.
- [8] X. Glorot and Y. Bengio. Understanding the difficulty of training deep feedforward neural networks. In *AISTATS*, 2010.
- [9] I. Goodfellow, J. Pouget-Abadie, M. Mirza, B. Xu, D. Warde-Farley, S. Ozair, A. Courville, and Y. Bengio. Generative adversarial nets. In *NIPS*, 2014.
- [10] A. Gretton, K.M. Borgwardt, M.J. Rasch, B. Scholkopf, and A. Smola. A kernel two-sample test. *JMLR*, 2012.
- [11] Zhiting Hu, Zichao Yang, Ruslan Salakhutdinov, and Eric P. Xing. On unifying deep generative models. In *arXiv*, 2017.
- [12] D. Kingma and J. Ba. Adam: A method for stochastic optimization. In *ICLR*, 2015.
- [13] D. P. Kingma and M. Welling. Auto-encoding variational Bayes. In *ICLR*, 2014.
- [14] A. Makhzani, J. Shlens, N. Jaitly, I. Goodfellow, and B. Frey. Adversarial autoencoders. *arXiv:1511.05644v2*, 2016.
- [15] L. Mescheder, S. Nowozin, and A. Geiger. Adversarial variational bayes: Unifying variational autoencoders and generative adversarial networks. In *arXiv*, 2016.
- [16] Y. Mroueh and T. Sercu. Fisher GAN. *arXiv:1705.09675v2*, 2017.
- [17] Y. Mroueh, T. Sercu, and V. Goel. Mcgan: Mean and covariance feature matching GAN. *arXiv:1702.08398v2*, 2017.
- [18] A. Muller. Integral probability metrics and their generating classes of functions. *Advances in Applied Probability*, 1997.
- [19] A. Oord, N. Kalchbrenner, and K. Kavukcuoglu. Pixel recurrent neural network. In *ICML*, 2016.
- [20] A. Radford, L. Metz, and S. Chintala. Unsupervised representation learning with deep convolutional generative adversarial networks. In *ICLR*, 2016.
- [21] D.J. Rezende and S. Mohamed. Variational inference with normalizing flows. In *ICML*, 2015.
- [22] T. Salimans, I. Goodfellow, W. Zaremba, V. Cheung, A. Radford, and X. Chen. Improved techniques for training gans. In *NIPS*, 2016.
- [23] T. Salimans, A. Karpathy, X. Chen, and D. P. Kingma. Pixelcnn++: Improving the pixelcnn with discretized logistic mixture likelihood and other modifications. In *ICLR*, 2017.

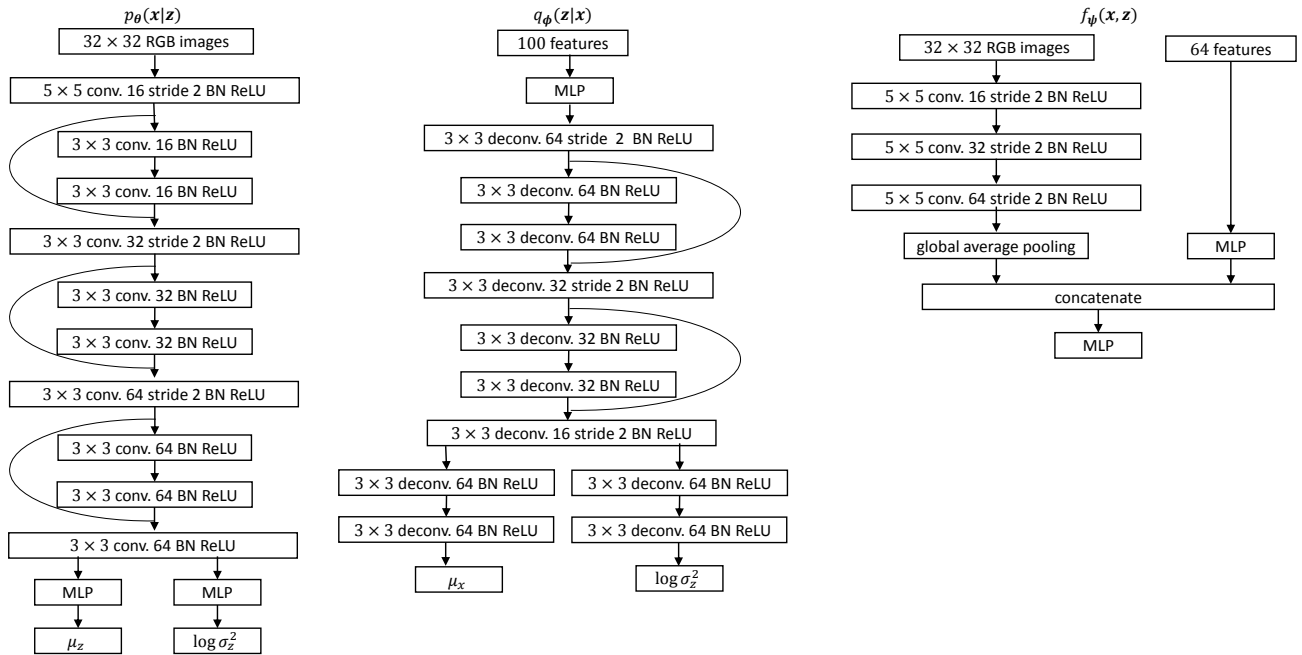
- [24] N. Srivastava, G. Hinton, A. Krizhevsky, I. Sutskever, and R. Salakhutdinov. Dropout: A simple way to prevent neural networks from overfitting. *JMLR*, 2014.
- [25] M.E. Tipping and C.M. Bishop. Probabilistic principal component analysis. *Journal of the Royal Statistical Society, Series B*, 61:611–622, 1999.
- [26] H.L. Van Trees. Detection, estimation, and modulation theory. In *Wiley*, 2001.
- [27] P. Vincent, H. Larochelle, I. Lajoie, Y. Bengio, and P.-A. Manzagol. Stacked denoising autoencoders: Learning useful representations in a deep network with a local denoising criterion. *JMLR*, 2010.
- [28] J. Zhao, M. Mathieu, and Y. LeCun. Energy-based generative adversarial network. *ICLR*, 2016.
- [29] J. Zhao, M. Mathieu, and Y. LeCun. Energy-based generative adversarial network. In *ICLR*, 2017.
- [30] J. Zhu, T. Park, P. Isola, and A. Efros. Unpaired image-to-image translation using cycle-consistent adversarial networks. In *arXiv:1703.10593*, 2017.

A Model Architectures

A.1 Model Architecture for MNIST



A.2 Model Architecture for CIFAR



A.3 Model Architecture for ImageNet

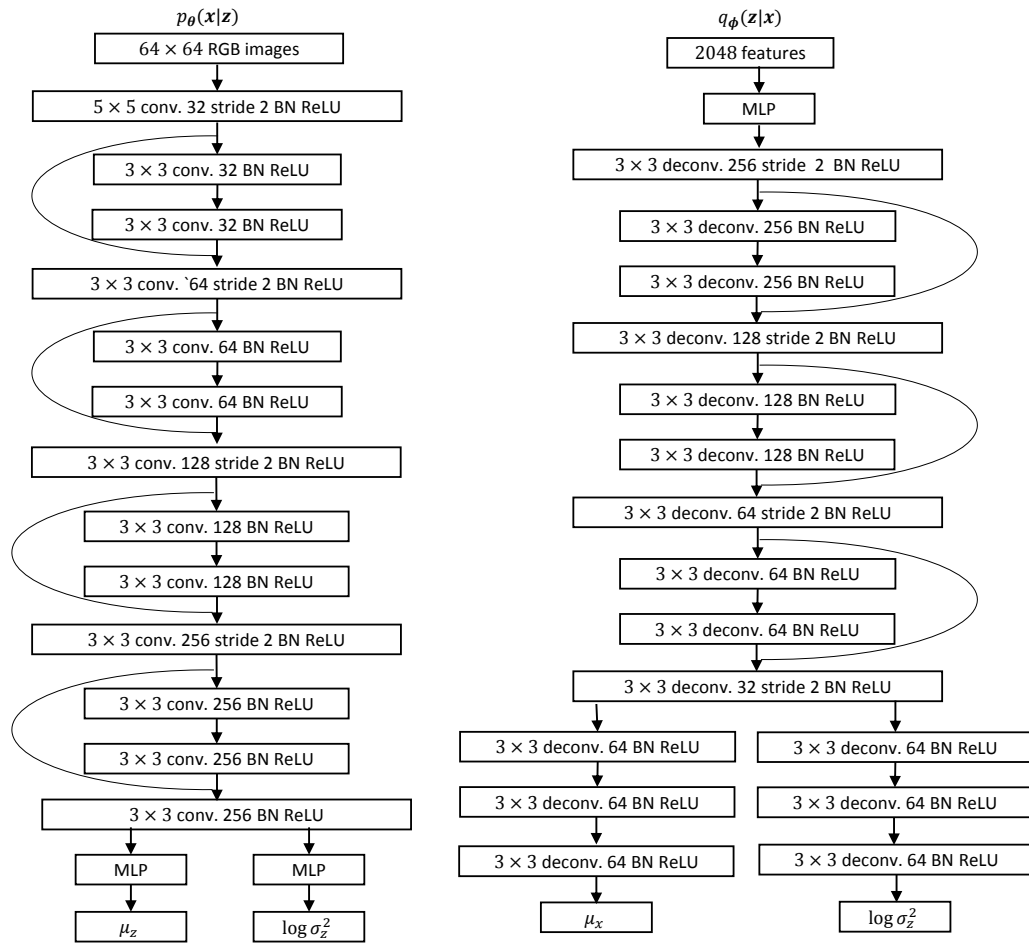


Figure 7: Encoder and decoder for ImageNet

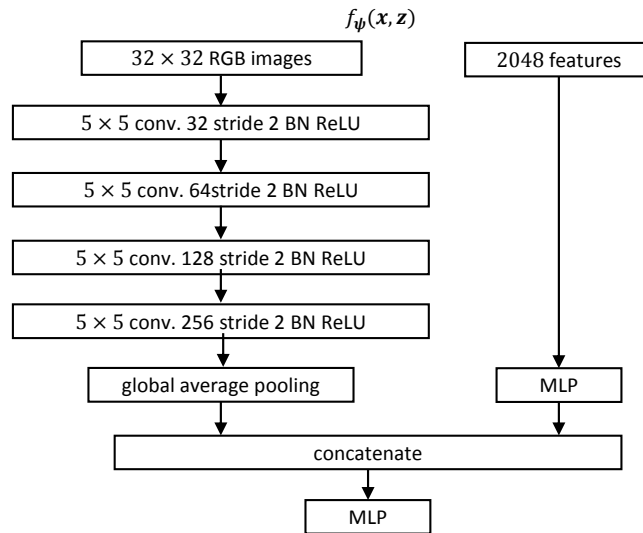


Figure 8: Discriminator for ImageNet